WEP Warwick Evans Publishing

International Journal of Materials Science and Technology Studies

ISSN: 3006-7693 (Print), ISSN: 3006-3744 (Online) | Volume 5, Number 2, Year 2026
DOI: https://doi.org/10.62051/ijmsts.v5n2.06
Journal homepage: https://wepub.org/index.php/IJMSTS/index

Study on the Laser Wire Filling Welding Process and Properties of 6061-T6 Aluminum Alloy Lap Joints

Shuming Zhang *, Yi Zhong, Jun Lu, Jipeng Zhu, Yuquan Wu

School of Materials and Chemistry, University of Shanghai for Science and Technology, Shanghai 200093, PR China

*Corresponding Author: Shuming Zhang

ABSTRACT

This study systematically investigates the laser wire filling welding (LWFW) process of 6061-T6 aluminum alloy lap joints using ER5356 filler wire. The influence of critical process parameters, including laser power, welding speed, and wire feed speed, on weld formation, microstructural evolution, and mechanical properties was evaluated. The results demonstrate that line energy input, determined by laser power and welding speed, is the primary factor governing penetration depth and macroscopic quality. An increase in laser power significantly enhances penetration by stabilizing the keyhole effect, while higher welding speeds refine the Heat-Affected Zone (HAZ) grains by reducing thermal residence time. Microstructural analysis revealed distinct zoning, with fine equiaxed grains in the weld metal (WM) and columnar crystals near the fusion line. The tensile strength of the joints is determined by the synergy between the effective bonding area (penetration depth) and fine-grain strengthening. Under the optimized conditions of 2.8 kW laser power, 25 mm/s welding speed, and 4.0 m/min wire feed speed, high-quality joints with a tensile strength of 195 MPa (approximately 63% of the base metal strength) were obtained. This research provides a theoretical and technical basis for the application of LWFW in automotive aluminum component manufacturing.

KEYWORDS

6061 aluminum alloy; Laser wire filling welding (LWFW); Microstructure; Tensile strength; Process optimization

1. INTRODUCTION

The increasingly stringent environmental protection standards are propelling the global automotive industry toward a strategic transformation characterized by lightweight design and low-emission profiles [1]. Due to their exceptional specific strength, excellent formability, superior thermal conductivity, and corrosion resistance, aluminum alloys have emerged as pivotal materials for automotive lightweighting. Currently, the application of aluminum alloys in automotive hoods in North America has reached 45%, with a projected increase to 85% by 2025 [2, 3]. Leading automakers, such as Honda, have already achieved weight reductions of over 20 kg per vehicle through the implementation of aluminum components [4]. Among these, 6061 aluminum alloy, a heat-treatable Al-Mg-Si alloy, is extensively utilized in structural components [5]. Consequently, the advancement of its welding technology directly determines the engineering efficacy of aluminum alloy assemblies [6, 7].

Traditional welding techniques, such as Tungsten Inert Gas (TIG) and Metal Inert Gas (MIG) welding, are technically mature and utilize relatively simple equipment [8, 9]. However, they are fraught with challenges, including high heat input, significant thermal distortion, and a high susceptibility to

solidification cracking and porosity. These limitations make it difficult to meet the modern automotive industry's requirements for high production cycles, large-scale automation, and superior part consistency [10, 11]. In contrast, laser welding has become a critical technology for automotive aluminum components due to its concentrated energy density, high processing speeds, minimal heat input, and narrow Heat-Affected Zone (HAZ) [12]. Nevertheless, the widespread industrial application of laser welding to aluminum alloys faces substantial obstacles, including the material's high reflectivity to laser beams, the vaporization of volatile alloying elements, and a high sensitivity to porosity and cracking. These issues are further exacerbated by the material's dense oxide layer, high thermal conductivity, low coefficient of thermal expansion, and low melting temperature [13, 14].

Laser wire filling welding (LWFW) serves as an optimized process that addresses these deficiencies by replenishing burnt-off alloying elements, suppressing solidification cracks, and bridging assembly gaps [15]. Despite its potential, the development of high-power laser welding equipment and associated process research in China started relatively late, resulting in a discernible gap compared to international benchmarks [16]. Specifically, research regarding the optimization of process parameters, the correlation between microstructure and mechanical properties, and the regulation of porosity in 6061 aluminum alloy lap joints remains insufficient [17].

Building upon this context, the present study utilizes 6061 aluminum alloy as the base metal and ER5356 alloy as the filler wire to conduct laser wire filling welding experiments on lap joints. This research systematically investigates the effects of process parameters-namely laser power, welding speed, and wire feed speed-on weld morphology and penetration depth. Furthermore, the microstructural characteristics and precipitate compositions of the welded joints are analyzed to explore the correlation between process parameters and the resulting microhardness and tensile properties. Additionally, the role of the lap gap in regulating porosity and mechanical performance is examined. By determining the optimal welding parameters, this study aims to provide a theoretical foundation and technical reference for the engineering application of laser wire filling welding in automotive aluminum component manufacturing, while simultaneously contributing to the localized advancement of laser welding technologies.

2. EXPERIMENTAL MATERIALS AND METHODS

2.1. Experimental Materials and Specimen Preparation

In this study, 6061-T6 aluminum alloy plates with thicknesses of 2 mm and 3 mm were utilized. The welding was performed in a lap joint configuration, with the 2 mm and 3 mm plates serving as the upper and lower sheets, respectively, while the assembly gap was maintained at 0 mm. An ER5356 aluminum alloy filler wire with a diameter of 1.2 mm was selected for the welding process. The dimensions of the test plates were 100 mm × 50 mm.

Prior to welding, to eliminate the adverse effects of the surface oxide film and impurities on the welding quality, the weld zones were mechanically ground until a metallic luster was exposed. Subsequently, the specimens were ultrasonically cleaned in acetone and dried for further use.

Table 1. Chemical compositions of 6061 aluminum alloy and ER5356 filler wire

	Mg	Si	Cu	Mn	Fe	Zn	Cr	Al
6061 (wt%)	1.1	0.72	0.21	0.09	0.4	0.02	/	other
ER5356 (wt%)	4.50-5.50	0.25	0.1	0.05-5.50	0.4	0.1	0.05-0.20	other

Table 2. Mechanical properties of the 6061 aluminum alloy used in the experiments

Property	Yield Strength σ_s(MPa)	Tensile Strength σ_b(MPa)	Density g/cm^3
Index	276	310	2.7

2.2. Welding Equipment

The laser wire filling welding experiments were conducted using an IPG YLR-4000 fiber laser with a rated power of 4 kW. The system integrated a KUKA KR210 industrial robot and a dedicated Fronius wire feed system, as illustrated in Figure 1. The fiber-delivered laser beam produced a circular spot with a diameter of 1.5 mm at the focal plane. During the welding process, high-purity argon (99.99%) was employed as the shielding gas, with the flow rate maintained at 15 L/min.

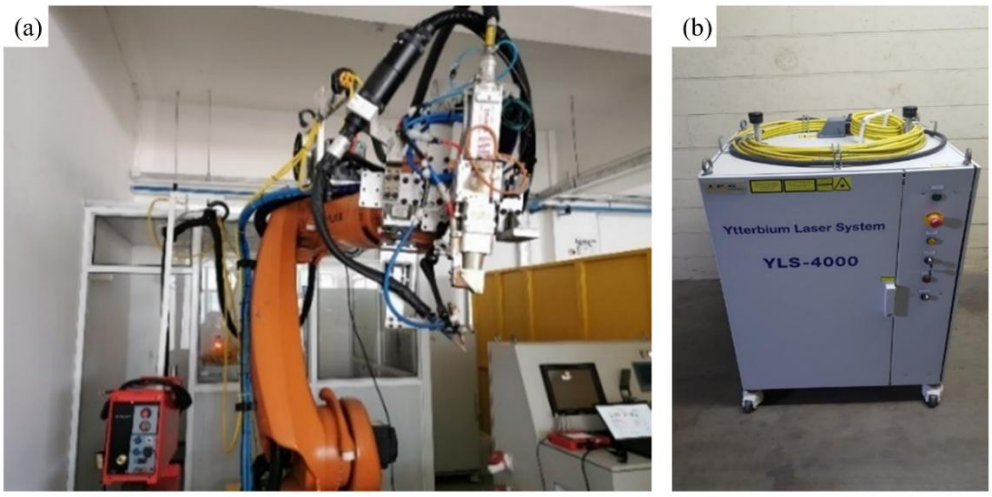

Figure 1. Schematic diagram of the welding apparatus

Prior to welding, to eliminate the adverse effects of the surface oxide film and impurities on the welding quality, the weld zones were mechanically ground until a metallic luster was exposed. Subsequently, the specimens were ultrasonically cleaned in acetone and dried for further use.

2.3. Welding Process and Experimental Design

The control variable method was employed to systematically investigate the influence of process parameters on weld formation regularities. The experimental parameters were varied within the following ranges: laser power (P) from 2.0 to 3.0 kW, welding speed (v_w) from 15 to 35 mm/s, and wire feed speed (v_f) from 3.0 to 5.0 m/min. The laser welding process is schematically depicted in Figure 2. The inclination angle of the filler wire relative to the horizontal substrate was set at 30°, adopting a front-feeding (leading) wire configuration. The defocusing distance was maintained at 0 mm throughout the experiments.

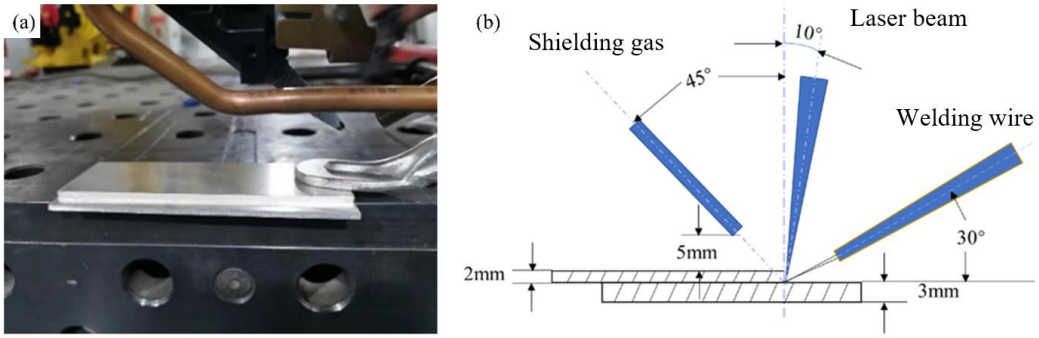

Figure 2. Schematic of the laser wire filling welding process

2.4. Performance Characterization and Microstructural Analysis

To systematically evaluate the formation quality and mechanical properties of the laser-welded joints, multi-scale characterization and testing were conducted. First, a Xiris XVC-1000 high-speed camera and WeldStudio software were employed to monitor the welding process, with a primary focus on analyzing the morphological characteristics of the metal vapor plume (plume) at the peak current moment under various power levels. Post-welding, macro-cross-sections of the welds were observed using a Leica S9i stereomicroscope to measure the penetration depth and quantify defects such as porosity.

Regarding microstructural analysis, a combination of a Keyence VHX-500F optical microscope (OM) and a Quanta 450 scanning electron microscope (SEM, 15 kV acceleration voltage) equipped with Energy Dispersive Spectroscopy (EDS) was utilized to characterize the phase composition, precipitate morphology, and element distribution behavior in the fusion zone and near the fusion line.

For mechanical property testing, a DHV-1000Z hardness tester was used to measure the microhardness distribution across the joint cross-section under a load of 0.98 N and a dwell time of 15 s, with a step size of 0.5 mm perpendicular to the weld. Simultaneously, tensile tests were performed on a Zwick/Roell Z050 universal testing machine at a crosshead speed of 1 mm/min. Mechanical data were recorded and correlated with SEM fractographic analysis to reveal the fracture and failure mechanisms of the joints.

3. RESULTS AND DISCUSSION

3.1. Dynamic Evolution Analysis of the Welding Process

High-speed imaging technology was utilized to capture the stable stage of the welding process at a sampling frequency of 5.5 Hz (approximately one frame every 0.18 s), providing a comprehensive record from wire melting to its entry into the molten pool. As shown in Figure 3, the laser wire filling welding process can be divided into three typical stages.

During the arc-striking and preheating stage (Fig. 3a-b), the tip of the filler wire first makes contact with the base metal surface, where it absorbs energy under the initial thermal radiation of the laser, resulting in preliminary melting. As energy continues to accumulate, the process enters the molten pool formation and stable filling stage (Fig. 3c-d), during which the filler wire and the base metal undergo intense simultaneous melting to form a dynamic molten pool. Under high laser energy density, a "keyhole" effect is generated, allowing the laser energy to be transmitted deep into the material through multiple reflections inside the keyhole [15]. At this point, the molten filler metal enters the pool under the influence of gravity and molten pool flow, effectively compensating for the element burn-off caused by the evaporation of the aluminum alloy. Finally, as the laser beam advances into the solidification and formation stage (Fig. 3e-f), the rear of the molten pool loses heat rapidly and solidifies under the influence of the shielding gas flow and substrate thermal conduction, forming a continuous weld with a specific ripple texture.

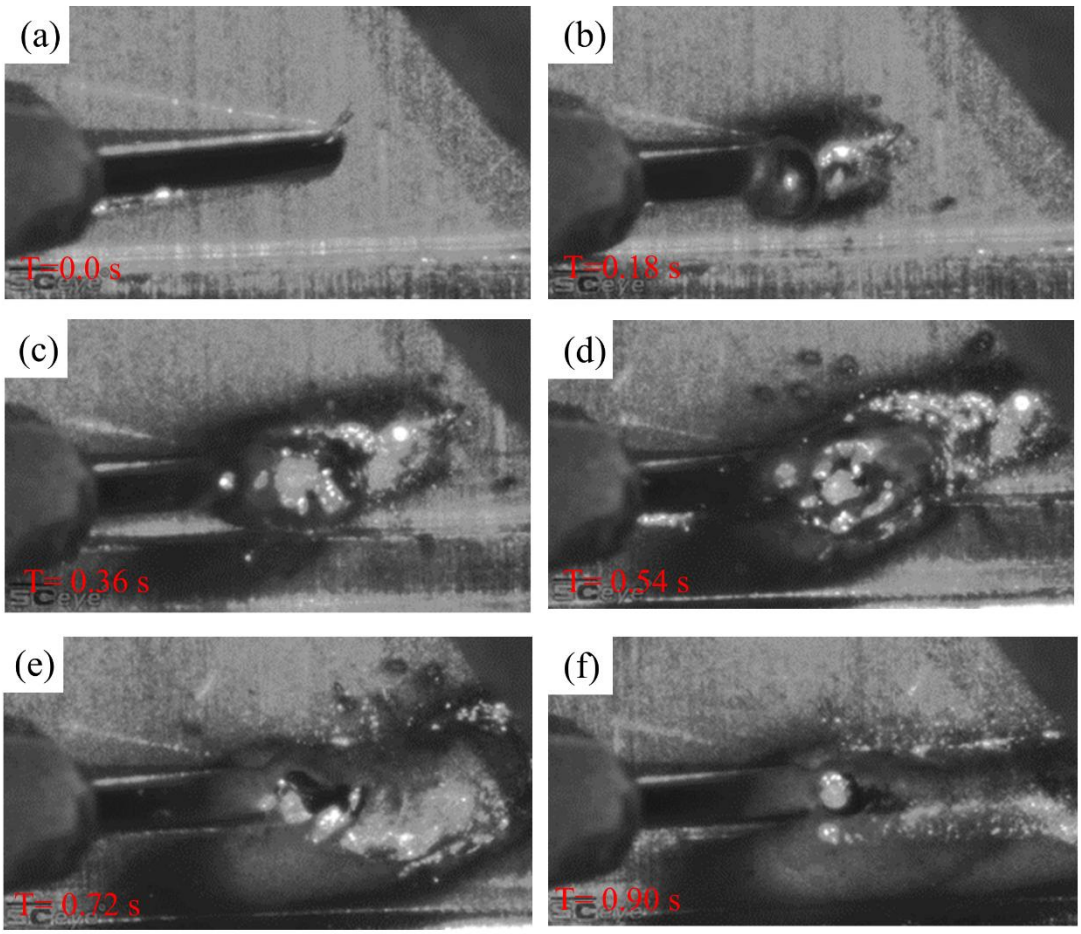

Figure 3. High-speed images of the dynamic evolution of the laser wire filling welding process: (a) t=0; (b) t=0.18s; (c) t=0.36s; (d) t=0.54s; (e) t=0.72s; (f) t=0.90s

3.2. Comprehensive Effects of Process Parameters on Weld Formation and Penetration Depth

3.2.1. Influence of Laser Power

Under fixed parameters (v_w = 25 mm/s, v_f = 4.0 m/min), the influence of laser power P on the weld morphology is illustrated in Figure 4. When P < 2.6 kW, the line energy obtained per unit length of the weld is insufficient, leading to inadequate heat exchange between the filler wire and the base metal. This results in poor wettability, uneven surface formation, and blurred textures. As the power increases to the 2.6 ~ 3.0 kW range, the sufficient heat input ensures full melting and wetting of both the wire and the substrate, yielding a well-filled weld with clear surface ripples and no significant defects such as cracks or undercuts.

Figure 5 demonstrates the effect of laser power on penetration depth. Observations indicate that within the 2.0 ~ 3.0 kW range, the penetration depth increases significantly with power, surging from 0.4 mm to 3.0 mm. Theoretical analysis suggests that the laser power directly determines the line energy input. Increased power enhances the stability of the keyhole effect, allowing the heat flow to penetrate deeper into the base metal. When the power reaches 3.0 kW, the heat input exceeds the thermal bearing capacity of the 6061 aluminum alloy plates, leading to direct burn-through.

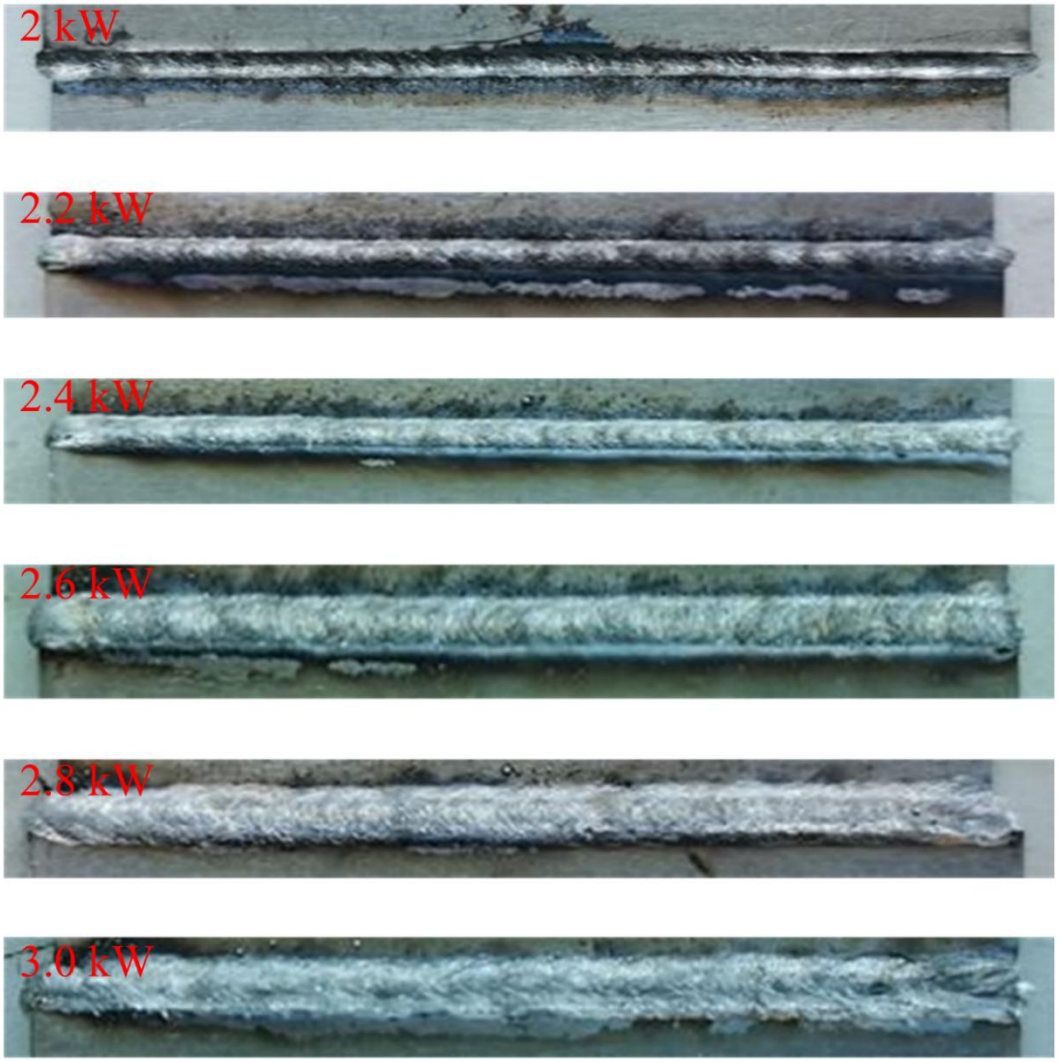

Figure 4. Influence of laser power on weld surface morphology: (a) 2 kW; (b) 2.2 kW; (c) 2.4 kW; (d) 2.6 kW; (e) 2.8 kW; (f) 3.0 kW.

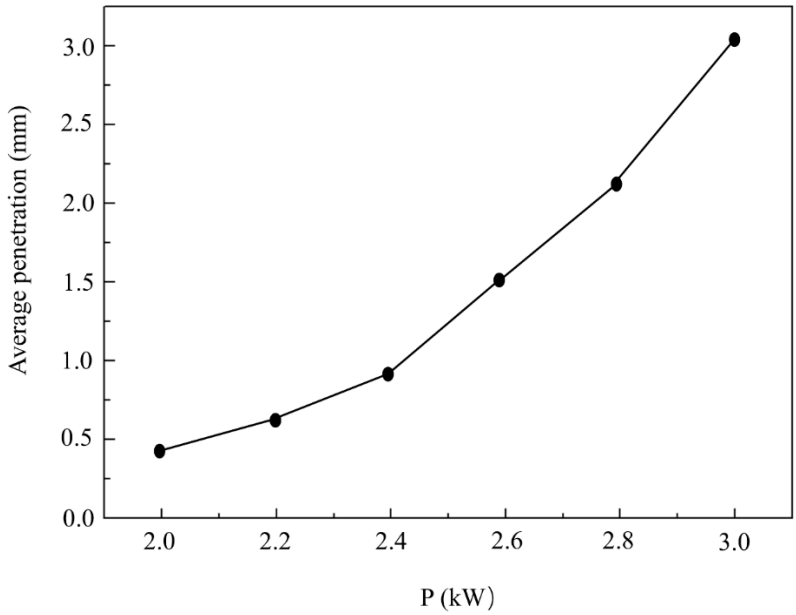

Figure 5. Curve of average penetration depth vs. laser power.

3.2.2. Influence of Welding Speed

The evolution of weld morphology and penetration depth as a function of welding speed v_w (ranging from 15 to 35 mm/s) under fixed parameters (P = 2.8 kW, v_f = 4.0 m/min) is shown in Figure 6. In the low-speed range (15 ~ 25 mm/s), the laser beam has a longer residence time per unit length, providing sufficient heat absorption for the weld metal. Consequently, the filler wire is fully melted, resulting in a weld with significant reinforcement and a large fusion width. As the speed increases to 25 ~ 35 mm/s, the heat input drops rapidly, and the wire melting and filling process becomes more hurried, leading to a simultaneous decrease in both reinforcement height and fusion width. At 35 mm/s, the mismatch between the welding speed and the wire feed speed causes a significant deterioration in formation quality, characterized by disordered and uneven textures.

Figure 7 shows that the penetration depth decreases approximately linearly with increasing welding speed (falling from 2.9 mm to 2.0 mm). Fundamentally, the welding speed reflects the duration of energy action. An increase in speed implies a shorter single-point irradiation time on the base metal, which reduces the melting efficiency of the metal within the pool and results in a shallower keyhole. This temporal effect of heat input directly constrains the deep-penetration capability of the molten pool.

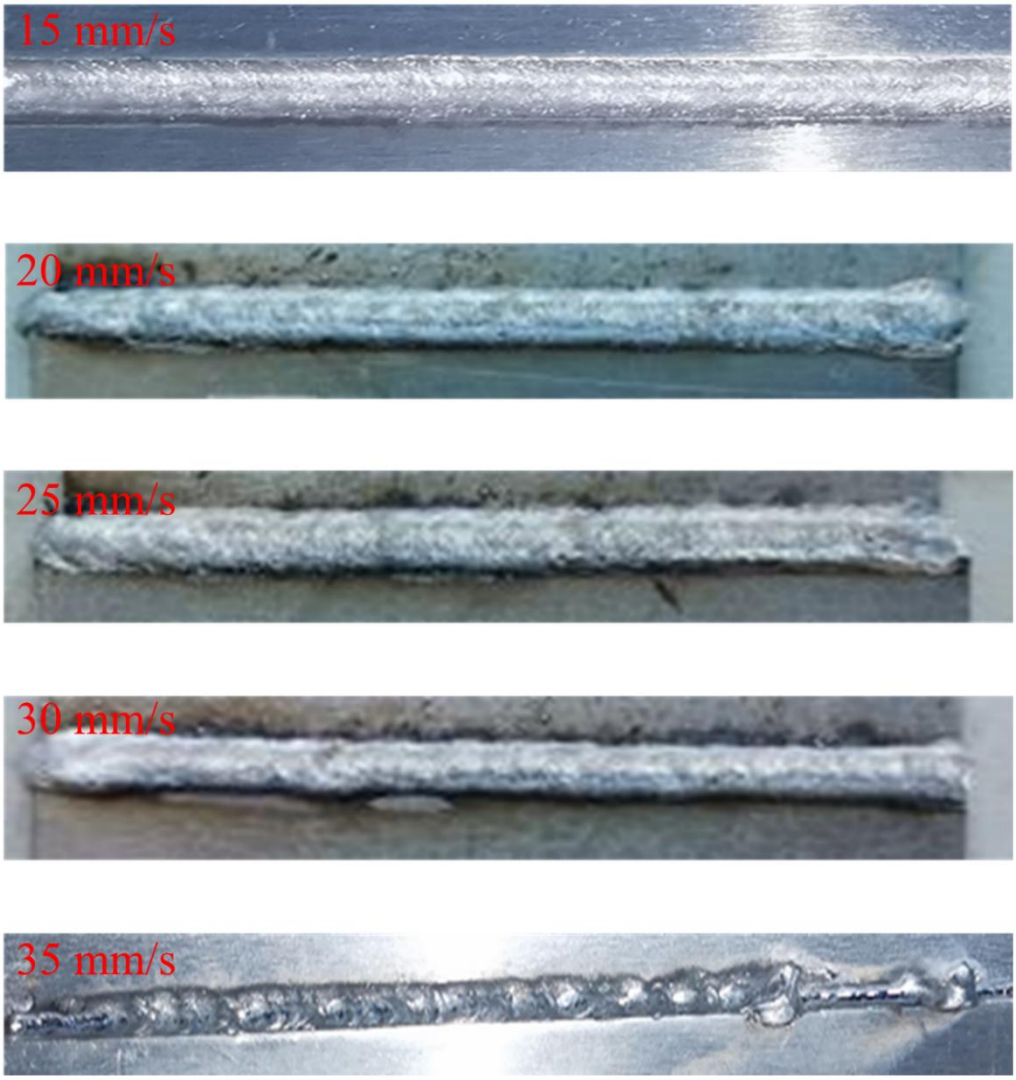

Figure 6. Influence of welding speed on weld surface morphology: (a) 15 mm/s; (b) 20 mm/s; (c) 25 mm/s; (d) 30 mm/s; (e) 35 mm/s.

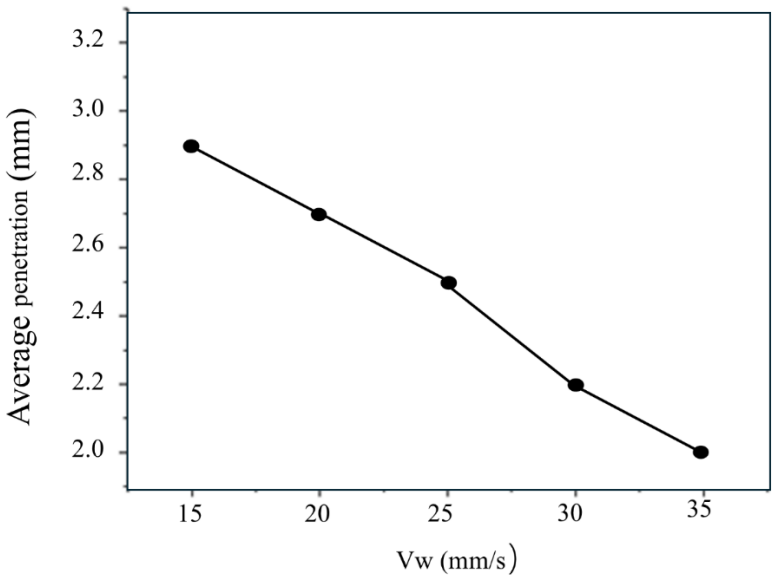

Figure 7. Curve of welding speed vs. average penetration depth.

3.2.3. Influence of Wire Feed Speed

The influence of wire feed speed v_f (3.0 ~ 5.0 m/min) on weld formation and penetration depth under fixed parameters (P = 2.8 kW, v_w = 25 mm/s) is depicted in Figure 8. As the wire feed speed increases, the fusion width of the weld shows no significant change. This is primarily because the laser power and spot diameter are fixed, meaning the dominant heat source determining the lateral expansion of the molten pool remains constant. However, the weld reinforcement increases significantly with the wire feed speed, leading to a more saturated formation and improved texture uniformity.

Figure 9 illustrates the effect of wire feed speed on penetration depth. Within the 3.0 ~ 4.5 m/min range, the penetration depth remains relatively stable, fluctuating around 2 mm without significant increase or decrease. Theoretically, changes in wire feed speed primarily affect the mass flux of the filler metal without altering the total line energy input to the base metal. Given constant laser power and spot characteristics, the effective heat absorbed by the base metal remains constant. Therefore, the increase in wire feed speed primarily manifests as an enhanced "filling effect," where more filler wire is melted and deposited on the surface, rather than altering the vertical penetration depth.

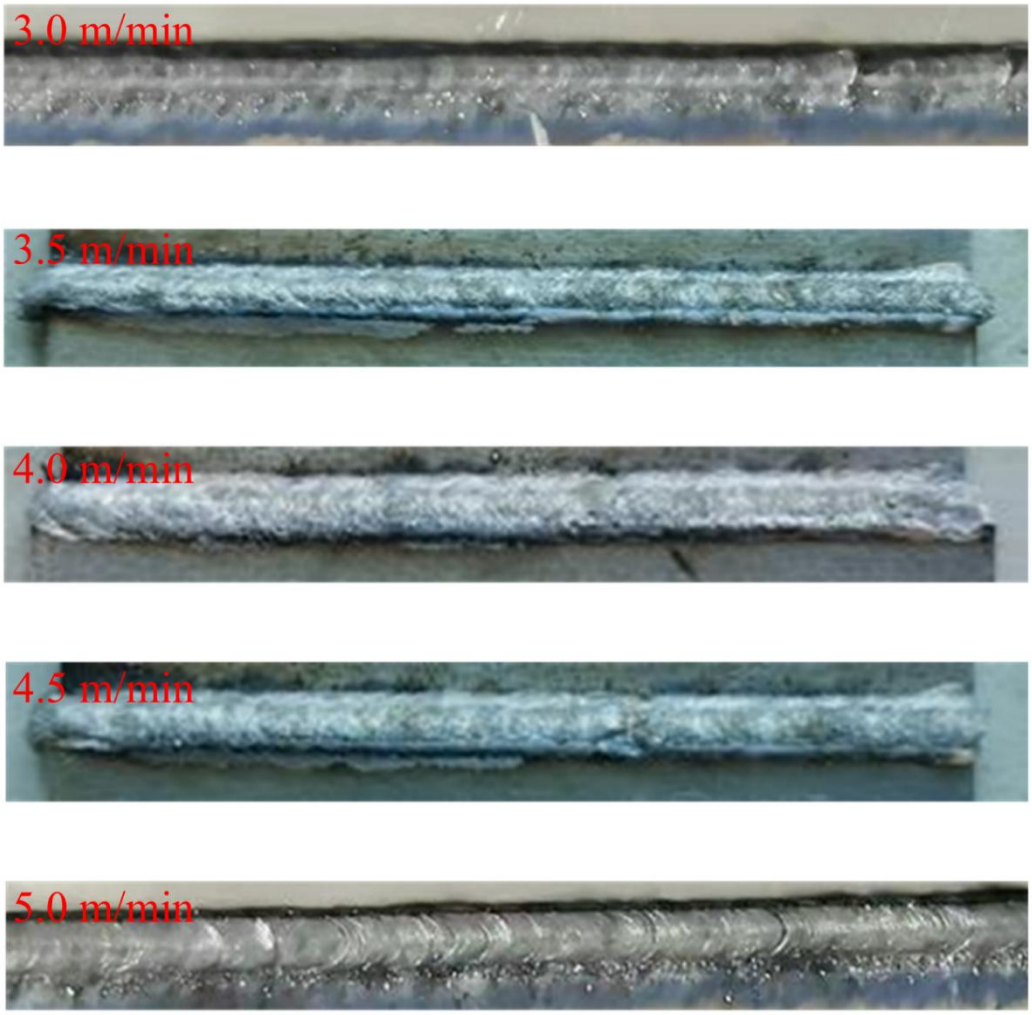

Figure 8. Influence of wire feed speed on weld surface morphology: (a) 3.0 m/min; (b) 3.5 m/min; (c) 4.0 m/min; (d) 4.5 m/min; (e) 5.0 m/min.

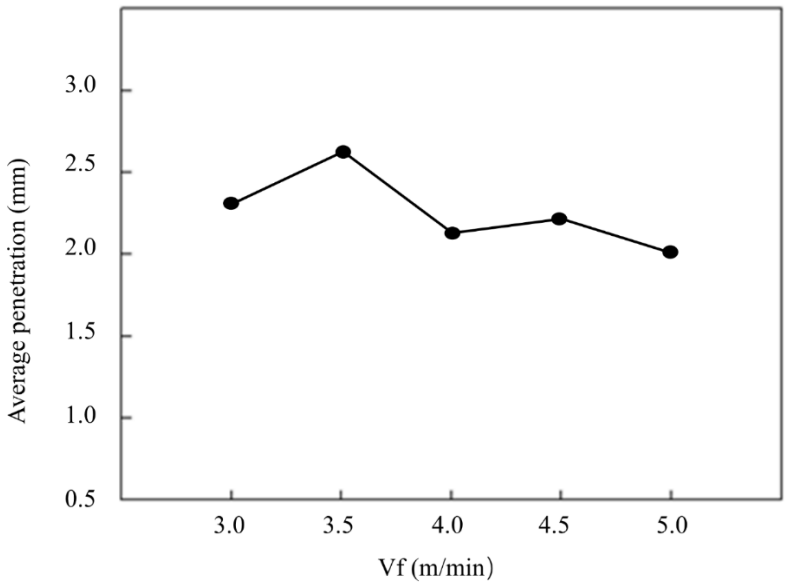

Figure 9. Wire feed speed vs. average weld penetration depth.

3.3. Microstructural Characteristics

3.3.1. Microstructural Zoning

The microstructure of a welded joint is the core factor determining its mechanical properties. The laser wire filling welded joint of 6061 aluminum alloy can be divided into four distinct characteristic regions: the Base Metal (BM), the Heat-Affected Zone (HAZ), the Fusion Line (FL), and the Weld Metal (WM). This section systematically analyzes the regulation laws of laser power, welding speed, and wire feed speed on the HAZ width and grain size, supported by XRD analysis to clarify the phase composition of the weld, providing a micro-mechanism foundation for subsequent mechanical property studies.

3.3.2. Influence of Laser Power

The microstructure of the 6061 aluminum alloy base metal consists of coarse as-rolled equiaxed grains with an average grain size of approximately 40 μm and a small amount of dispersed precipitates on the matrix. After laser wire filling welding, the fusion line is clearly visible. The HAZ region near the fusion line exhibits slight grain growth compared to the base metal due to the laser thermal cycle. Near the fusion line, columnar crystals grow perpendicular to the fusion line direction. This is because, during the laser welding process, heat dissipation is fastest along the fusion line direction, creating the maximum temperature gradient and causing grains to grow preferentially along the heat flow direction.

The weld center consists of fine and uniform equiaxed grains, a phenomenon resulting from two factors: first, the rapid heating and cooling characteristics of laser welding inhibit grain growth; second, the mechanical stirring of the filler wire and the impact of the droplets on the molten pool break up the primary dendrites, promoting the formation of new nucleation sites, which eventually grow into fine equiaxed grains. Compared to traditional welding, LWFW has a smaller heat input and higher welding speed, significantly reducing the thermal effect on the HAZ, effectively inhibiting grain coarsening, and resulting in a narrower HAZ, which helps reduce welding distortion and the risk of solidification cracking.

Based on these microstructural features, laser powers of 2.0 kW and 2.8 kW (at v_w=25 mm/s, v_f=4.0 m/min) were selected to investigate their impact on the HAZ and grain size (Fig. 10). Results show that at 2.0 kW, the HAZ is narrower and the weld grains are finer, with an average size of ~ 25 μm. When the power increases to 2.8 kW, the HAZ width increases significantly, and the grain size coarsens noticeably to ~ 33 μm. The core mechanism is that laser power determines the heat input: at lower power, the insufficient heat input limits the heating range of the HAZ and the thermodynamic driving force for grain growth is weak; at higher power, the significantly increased heat input extends the high-temperature residence time in the HAZ, allowing for full grain growth. Since grain coarsening can weaken joint performance, the laser power must be optimized to avoid excessive values while ensuring sufficient penetration.

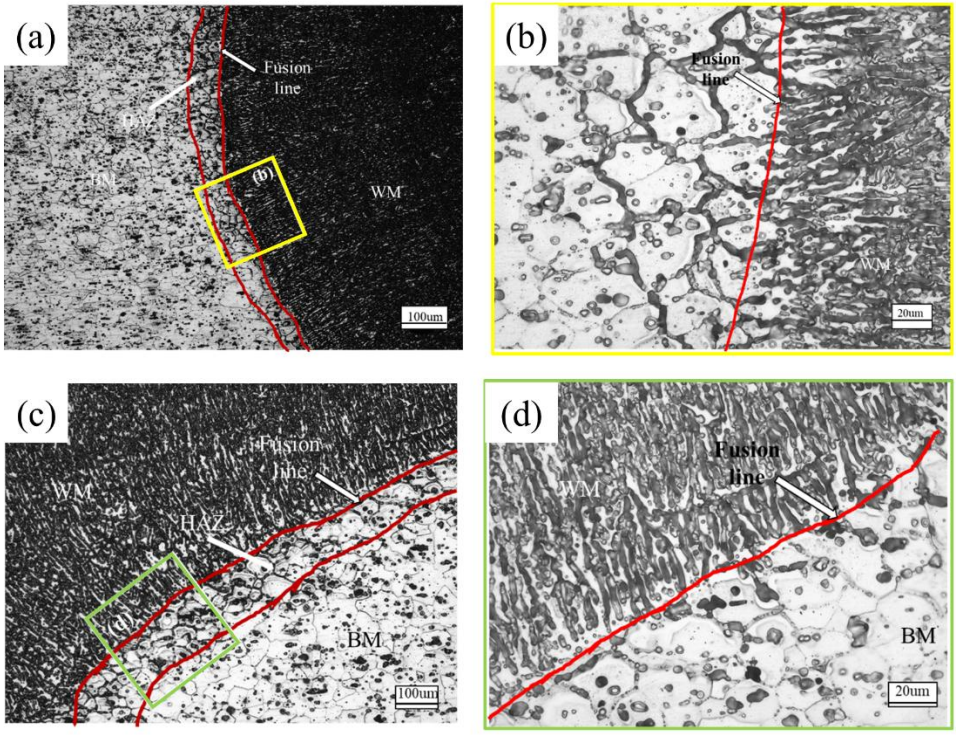

Figure 10. HAZ images under different laser powers: (a) 2.0 kW; (b) Enlarged view of the marked area in (a); (c) 2.8 kW; (d) Enlarged view of the marked area in (c).

3.3.3. Influence of Welding Speed

Welding speeds of 15 mm/s and 25 mm/s (at P=2.8 kW,v_f=4.0 m/min) were selected to analyze their impact on the HAZ and grain size (Fig. 11). The welding speed regulates heat input by changing the laser residence time on the weld. At 15 mm/s, the longer residence time results in sufficient heat input to the HAZ, allowing grains to grow fully, leading to a wider HAZ and larger grains (~ 28 μm), with more pronounced columnar crystal growth near the fusion line. When the speed increases to 25 mm/s, the residence time is shortened, heat input is reduced, and grain growth is inhibited. Consequently, the HAZ narrows significantly, and grains are refined to ~ 22 μm with more fine and uniform equiaxed grains in the weld center. Fine grain strengthening is a vital mechanism for improving mechanical properties; thus, appropriately increasing the welding speed helps refine the microstructure and narrow the HAZ, further reducing distortion risks.

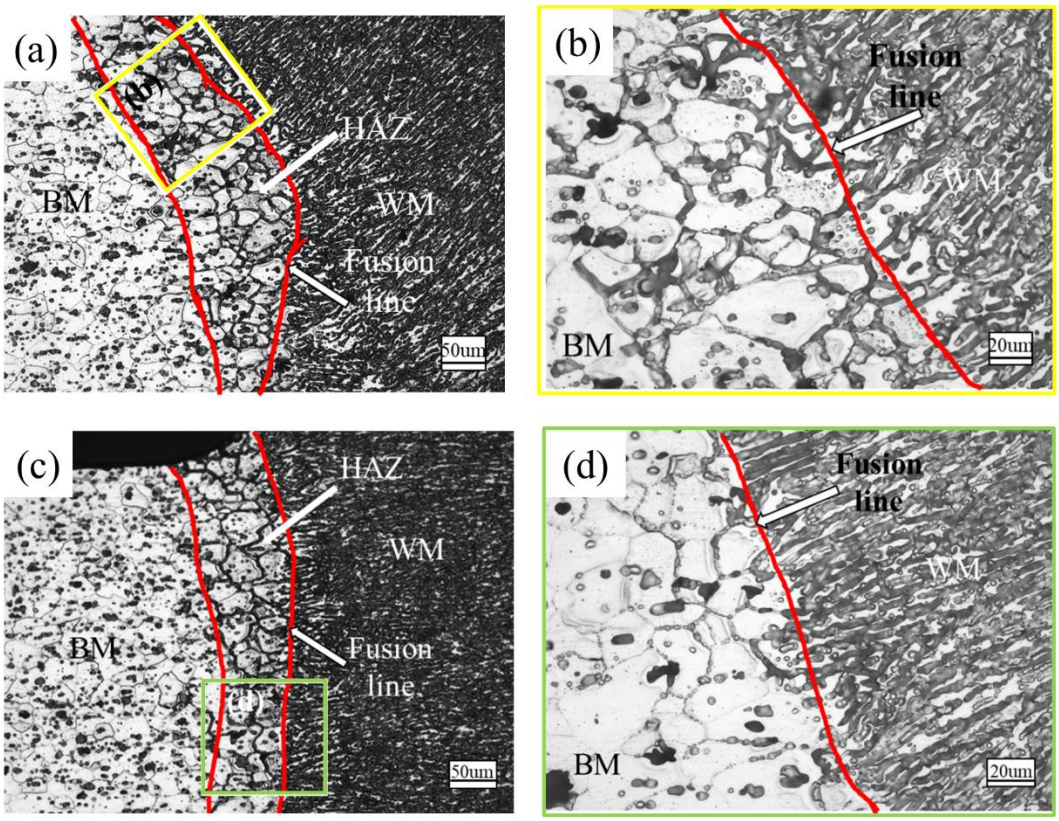

Figure 11. HAZ images under different welding speeds: (a) 15 mm/s; (b) Enlarged view of the marked area in (a); (c) 25 mm/s; (d) Enlarged view of the marked area in (c).

3.3.4. Influence of Wire Feed Speed

Wire feed speeds of 3.0 m/min and 4.0 m/min (at P=2.8 kW, v=25 mm/s) were selected (Fig. 12). Results show no significant difference in the overall microstructural partitioning under both speeds, maintaining the pattern of coarse equiaxed grains in the BM, columnar crystals near the FL, and fine equiaxed grains in the WM center. The differences in HAZ width and grain size are minimal: ~ 21 μm at 3.0 m/min vs. ~ 19 μm at 4.0 m/min. This occurs because the wire feed speed does not alter the heat input conditions; with constant laser power and welding speed, the thermal cycle in the HAZ remains stable, leading to consistent grain growth and HAZ width. The wire feed speed primarily influences weld filling and reinforcement, with negligible effects on microstructure morphology and grain growth.

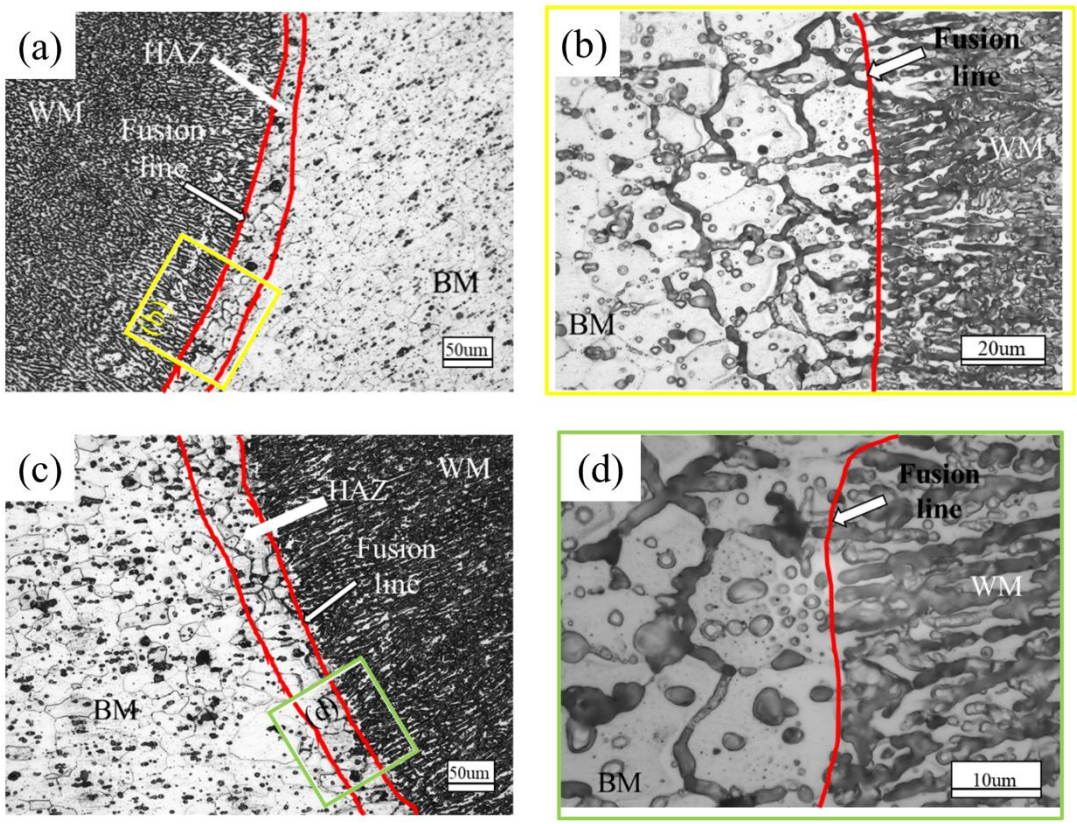

Figure 12. HAZ images under different wire feed speeds: (a) 3.0 m/min; (b) Enlarged view of the marked area in (a); (c) 4.0 m/min; (d) Enlarged view of the marked area in (c).

3.3.5. Weld Phase Composition Analysis (XRD)

To clarify the phase composition of the weld zone, XRD identification was performed on the welds for laser powers of 2.8 kW and 3.0 kW (at v_w = mm/s}, v_f = 4.0 m/min), as shown in Figure 13. The XRD patterns for the 6061 base metal and the samples exhibit characteristic diffraction peaks of the α-Al matrix, with no detection of the typical Mg_2Si strengthening phase of the 6061 alloy. This result is primarily attributed to: first, the maximum solubility of Mg_2Si in Al-Mg-Si alloys is only 1.73%, making its actual precipitation in the weld a trace second phase; second, the extremely high cooling rate of laser welding causes alloying elements to remain in solid solution within the aluminum matrix, inhibiting the full precipitation of strengthening phases; finally, the limited sensitivity of XRD for low-content phases means trace precipitates are easily masked by the intense matrix peaks. Therefore, subsequent high-magnification SEM-EDS observation is required to verify the distribution and morphology of the Mg_2Si phase.

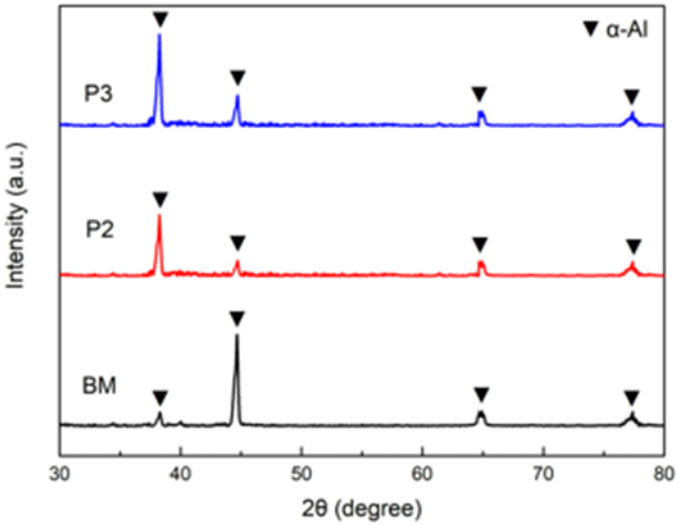

Figure 13. XRD patterns of the base metal and welds of samples P2 and P3.

3.4. Tensile Properties

Based on the previous findings regarding microstructure and process parameters, tensile tests were designed using the control variable method to analyze the impacts of laser power, welding speed, and wire feed speed on joint performance. All tensile specimens were sampled perpendicular to the weld direction, adhering to the GB/T 228.1-2010 standard, and tested at a rate of 1 mm/min on a universal testing machine. Observations revealed that all specimen fractures occurred at the weld metal (WM) center, indicating the weld zone as the weak link of the joint.

3.4.1. Influence of Laser Power on Strength

The influence of laser power on tensile performance is shown in Figure 14. At P=2.0 kW (v_w=25 mm/s, v_f=4.0 m/min), the joint tensile strength is only 140 MPa; when P increases to 2.8 kW, the strength significantly increases to 195 MPa, reaching 63% of the base metal strength.

Increased power has a dual effect on joint performance. On one hand, the increased heat input leads to grain coarsening in the HAZ (25 μm to 33 μm), which may weaken the microstructure; on the other hand, for lap joints, increasing power increases the penetration depth from 0.4 mm to 2.9 mm, greatly expanding the effective bonding area (i.e., metallurgical bonding interface) between the base metals. Since fracture occurs in the weld zone, the increase in bearing area due to greater penetration dominates the tensile strength, leading to better performance at higher power levels.

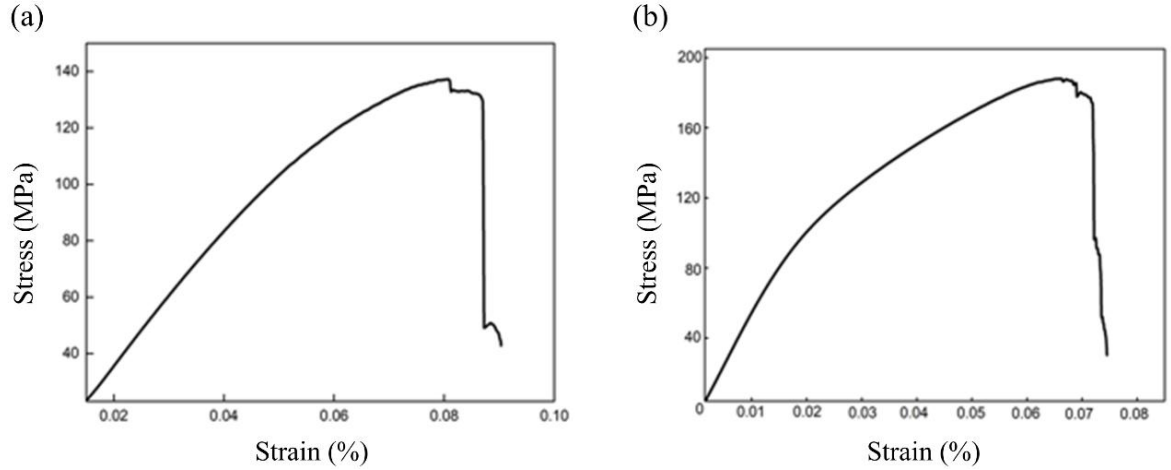

Figure 14. Stress-strain curves under different powers: (a) 2.0 kW; (b) 2.8 kW.

3.4.2. Influence of Welding Speed on Strength

The regulation of joint strength by welding speed is shown in Figure 15. At v_w=15 mm/s (P=2.8 kW, v_f=4.0 m/min), the tensile strength is 166 MPa; when increased to 25 mm/s, the strength rises to 191 MPa, approximately 62% of the base metal strength.

Welding speed primarily affects microstructural quality by altering the heating time. During high-speed welding, the laser line energy decreases, resulting in a narrower HAZ and significant grain refinement (28 μm to 22 μm). Although increased speed slightly reduces penetration, as long as full penetration (> 2 mm) is maintained, the contributions of fine grain strengthening and reduced thermal damage to joint strength are more prominent, making 25 mm/s the superior parameter for mechanical performance.

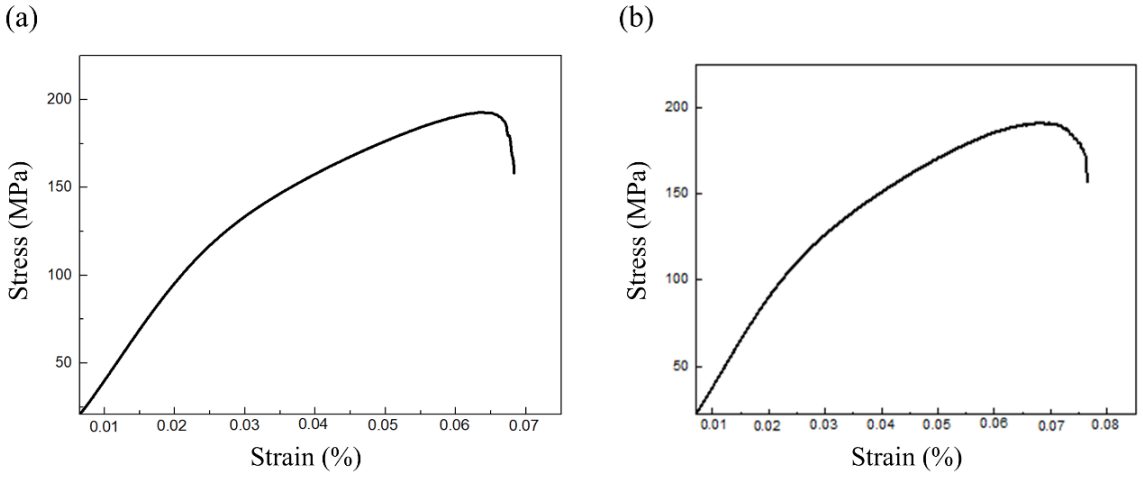

Figure 15. Stress-strain curves under different welding speeds: (a) 15 mm/s; (b) 25 mm/s.

3.4.3. Influence of Wire Feed Speed on Strength

As shown in Figure 16, changing the wire feed speed has a minimal impact on tensile performance. When v_f increases from 3.0 m/min to 4.0 m/min (at P = 2.8 kW, v=25 mm/s), the tensile strength only slightly decreases from 193 MPa to 190 MPa, a change of less than 2%. The essence of wire feed speed is to regulate the amount of filler metal, primarily affecting weld reinforcement and surface fullness. Since it does not significantly alter the effective heat input, it has almost no regulatory effect on HAZ characteristics or the critical penetration depth. With other parameters held constant, the internal metallurgical structure and bearing area remain stable, hence v_f has no significant influence on the final tensile strength.

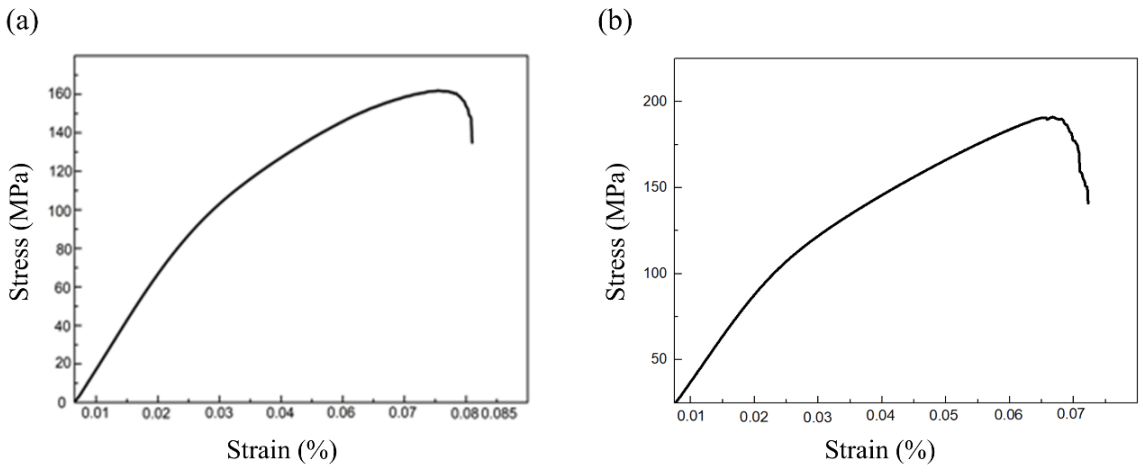

Figure 16. Stress-strain curves under different wire feed speeds: (a) 3.0 m/min; (b) 4.0 m/min.

4. CONFLICTS OF INTEREST

This study investigated the laser wire filling welding (LWFW) process of 6061 aluminum alloy lap joints. The main conclusions are as follows:

Line energy input (P and v_w) is the critical factor determining macroscopic weld quality. Penetration depth increases with laser power (0.4 to 3.0 mm) due to enhanced keyhole stability but decreases linearly with welding speed (2.9 to 2.0 mm). Wire feed speed primarily regulates weld reinforcement with negligible impact on penetration.

Joint microstructure exhibits distinct regional distribution, with equiaxed grains in the WM and columnar crystals at the FL. HAZ grain size is positively correlated with heat input (P increase coarsens grains from 25 to 33 μm; v increase refines them from 28 to 22 μm by shortening residence time).

Tensile strength is governed by the coupling of penetration depth (bonding area) and fine-grain strengthening. Optimal parameters (P=2.8 kW, v=25 mm/s, v_f=4.0 m/min) yielded a tensile strength of 195 MPa (~63% of base metal). Insufficient penetration leads to joint failure due to weak metallurgical bonding.

In conclusion, LWFW effectively improves welding defects in 6061 aluminum alloy. Precise heat input regulation through optimized matching of power and speed is essential for ensuring high-quality joints with adequate penetration.

REFERENCES

[1] Liu W, Peng T, Kishita Y, Umeda Y, Tang R, Tang W, et al. Critical life cycle inventory for aluminum die casting: A lightweight-vehicle manufacturing enabling technology. Applied Energy 2021; 304:117814. https://doi.org/10.1016/j.apenergy.2021.117814.

[2] Quoc TD, Lo Y-L, Raza MM, Chieh C-W, Chen C-Y, Tsai K-T. Optimization of blue laser welding for copper hairpins in EV motors. Journal of Materials Research and Technology 2026; 42:351–64. https://doi.org/10.1016/j.jmrt.2026.03.043.

[3] Gao Y-C, Dong B-X, Yang H-Y, Yao X-Y, Shu S-L, Kang J, et al. Research progress, application and development of high performance 6000 series aluminum alloys for new energy vehicles. Journal of Materials Research and Technology 2024; 32:1868–900. https://doi.org/10.1016/j.jmrt.2024.08.018.

[4] Kawajiri K, Kobayashi M, Sakamoto K. Lightweight materials equal lightweight greenhouse gas emissions? A historical analysis of greenhouse gases of vehicle material substitution. Journal of Cleaner Production 2020; 253:119805. https://doi.org/10.1016/j.jclepro.2019.119805.

[5] Chen Z, Li C, Li F, Li C. Enhancing the mechanical properties of 6061 aluminum alloy through the synergistic effects of twins, stacking faults, nanograins and lattice distortions. Journal of Materials Research and Technology 2025; 35:6650–8. https://doi.org/10.1016/j.jmrt.2025.02.242.

[6] Observation of Arc Behaviour in TIG/MIG Hybrid Welding Process - IOPscience n.d. https://iopscience.iop.org/article/10.1088/1755-1315/596/1/012025 (accessed March 28, 2026).

[7] Recent advances in joining technologies of aluminum alloys: a review | Discover Materials | Springer Nature Link n.d. https://link.springer.com/article/10.1007/s43939-024-00155-w (accessed March 28, 2026).

[8] POWER MIG weld tech takes step forward with 360MP | Trailer Body Builders n.d. https://www.trailer-bodybuilders.com/fabrication/article/21744460/power-mig-weld-tech-takes-step-forward-with-360mp (accessed March 28, 2026).

[9] Simulation Study on Weld Formation in Full Penetration Laser + MIG Hybrid Welding of Copper Alloy | MDPI n.d. https://www.mdpi.com/1996-1944/13/23/5307 (accessed March 28, 2026).

[10] Initiation and growth mechanisms for weld solidification cracking - N. Coniglio, C. E. Cross, 2013 n.d. https://journals.sagepub.com/doi/abs/10.1179/1743280413Y.0000000020 (accessed March 28, 2026).

[11] Liu J, Kou S. Susceptibility of ternary aluminum alloys to cracking during solidification. Acta Materialia 2017; 125:513–23. https://doi.org/10.1016/j.actamat.2016.12.028.

[12] Advanced High-Strength Steels for Automotive Applications: Arc and Laser Welding Process, Properties, and Challenges | MDPI n.d. https://www.mdpi.com/2075-4701/12/6/1051 (accessed March 28, 2026).

[13] Zhao H, White DR, DebRoy T. Current issues and problems in laser welding of automotive aluminium alloys. International Materials Reviews 1999; 44:238–66. https://doi.org/10.1179/095066099101528298.

[14] Laser Beam and Laser-Arc Hybrid Welding of Aluminium Alloys | MDPI n.d. https://www.mdpi.com/2075-4701/11/8/1150 (accessed March 28, 2026).

[15] Jin X, Cheng Y, Zeng L, Zou Y, Zhang H. Multiple reflections and fresnel absorption of gaussian laser beam in an actual 3D keyhole during deep-penetration laser welding. International Journal of Optics 2012; 2012:1–8. https://doi.org/10.1155/2012/361818.

[16] Advances in narrow linewidth diode lasers n.d. https://cdn.sciengine.com/doi/10.1007/s11432-019-9870-0 (accessed March 28, 2026).

[17] Fang J, Zhu Z, Zhang X, Xie L, Huang Z. Tensile deformation and fracture behavior of AA5052 aluminum alloy under different strain rates. J of Materi Eng and Perform 2021; 30:9403–11. https://doi.org/10.1007/s11665-021-06112-5.